

Molecular Dynamics of Potential rRNA Binders: Single-Stranded Nucleic Acids and Some Analogues

Joanna Panecka,^{†,‡} Cameron Mura,[§] and Joanna Trylska^{*,‡}

Department of Biophysics, Institute of Experimental Physics, Interdisciplinary Centre for Mathematical and Computational Modelling, University of Warsaw, Zwirki i Wigury 93, 02-089 Warsaw, Poland, and Department of Chemistry, University of Virginia, Charlottesville, Virginia 22904-4319, United States

Received: July 11, 2010; Revised Manuscript Received: November 11, 2010

By hindering or “silencing” protein translation *in vivo*, antisense nucleic acid analogues that hybridize to bacterial rRNA could serve as a promising class of antibacterial compounds. Thus, we performed a comparative analysis of the dynamical properties of modified oligonucleotides based upon a sequence ${}^5\text{r}(\text{U}\text{G}\text{U}\text{U}\text{A}\text{C}\text{G}\text{A}\text{C}\text{U}){}^3$ that is complementary to bacterial ribosomal A-site RNA. In particular, 25 ns explicit solvent molecular dynamics simulations were computed for the following six single-stranded decamers: (1) the above RNA in unmodified form; (2) the 2'-*O*-methyl-modified RNA; (3) peptide nucleic acid (PNA) analogues of the above sequence, containing either (a) T or (b) U; and (4) two serine-substituted PNAs. Our results show that 2'-*O*-methylation attenuates RNA backbone dynamics, thereby preventing interconversion between stacked and unstacked conformations. The PNA analogue is rendered less flexible by replacing uracil with thymine; in addition, we found that derivatizing the PNA backbone with serine leads to enhanced base-stacking interactions. Consistent with known solubility properties of these classes of molecules, both RNAs exhibited greater localization of water molecules than did PNA. In terms of counterions, the initially helical conformation of the 2'-*O*-methyl RNA exhibits the highest Na^+ density among all the simulated decamers, while Na^+ build-up was most negligible for the neutral PNA systems. Further studies of the conformational and physicochemical properties of such modified single-stranded oligomers may facilitate better design of nucleic acid analogues, particularly those capable of serving as specific, high-affinity ribosomal A-site binders.

1. Introduction

Antigene and antisense therapies use short oligonucleotide strands to target a complementary sequence of DNA or RNA, thereby inhibiting key biological processes of either RNA transcription¹ or protein translation.² Many nucleic acid analogues with potential antisense activity have been designed.^{3,4} Most of these oligonucleotides feature modified backbones in order to enhance their hybridization to complementary segments of nucleic acid, their metabolic stabilities, or to reduce their toxicities. Modifications that have been synthesized thus far include the replacement of phosphates by phosphorothioates,⁵ the addition of a constraint stabilizing the sugar ring in the C3'-endo conformation,⁶ or substitution with various alkyl-based groups at the 2'*O* position.⁷ There are also classes of analogues wherein the ribophosphate backbone is entirely redesigned, as in the peptide nucleic acids (PNA).⁸ Some of these novel compounds are promising candidates for antiviral, anticancer, and antibacterial drugs.⁹ Antisense oligomers may be applied in gene silencing strategies against viral infections (e.g., hepatitis C¹⁰), or in interfering with reverse transcription in the case of HIV.¹¹ Antisense oligonucleotides can also attenuate aberrant gene expression,¹² such as occurs in many cancers. Finally, studies have also shown that interactions between antisense oligonucleotides and messenger RNA (mRNA) or ribosomal

RNA (rRNA) offer potential avenues to design sequence-specific antibiotics;¹³ in these applications, oligomers roughly ten nucleotides in length were found to be most effective.^{14,15} The study reported here focuses on decameric nucleic acid analogues with promising antibacterial activity.

The oligomers in our present study were chosen with sequences complementary to rRNA in the proximity of the aminoacyl-tRNA binding site (the A-site). This functionally important region of the small (30S) ribosomal subunit contains weakly paired and solvent-exposed nucleotides, and thus is readily accessible to sequence-specific binders. In previous experimental work, 2'-*O*-methyl ribonucleotide (2'-*O*-MeRNA) decamers were found to exhibit complementary pairing to rRNA segments of bacterial 30S subunits in the A-site region, with nano- to micromolar affinities.¹⁵ In particular, the 2'-*O*-MeRNA oligomer of sequence ${}^5\text{r}(\text{U}\text{G}\text{U}\text{U}\text{A}\text{C}\text{G}\text{A}\text{C}\text{U}){}^3$, complementary to residues 1493–1502 (according to the *Escherichia coli* standard numbering convention), was found to bind most tightly ($K_d = 29 \text{ nM}$). Thus, oligonucleotides based upon this sequence may provide a useful means to increase the specificity of clinically used aminoglycosidic antibiotics that bind to the A-site.¹⁶ A conceivable approach would be to covalently link aminoglycoside molecules to the oligonucleotides (or analogues thereof). Such attempts were reported for the aminoglycoside neamine, which was conjugated to PNA dimers;¹⁷ the tandem molecule was found to bind to the A-site rRNA fragment with similar affinity as neamine.

Given the experimental results alluded to above, 2'-*O*-MeRNA and PNA are two sets of modified nucleotides that warrant further consideration as specific rRNA binders and, therefore, potentially promising antisense compounds. The 2'-

* To whom correspondence should be addressed. E-mail: joanna@icm.edu.pl. Phone: +48 (22) 5540-843. Fax: +48 (22) 5540-801.

[†] Department of Biophysics, Institute of Experimental Physics, University of Warsaw.

[‡] Interdisciplinary Centre for Mathematical and Computational Modelling, University of Warsaw.

[§] Department of Chemistry, University of Virginia.

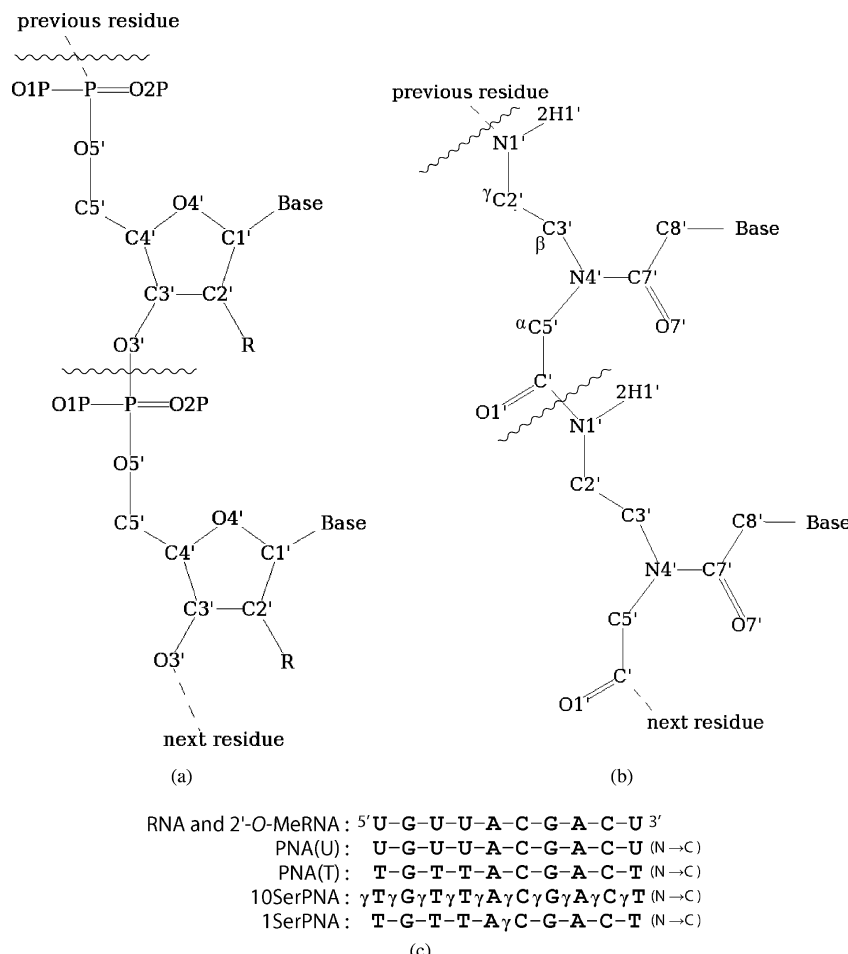


Figure 1. Schematic representations of the heavy atom backbones are shown for (a) RNA and 2'-O-MeRNA ($R = CM2$ for 2'-O-MeRNA and HO $2'$ for RNA), and (b) PNA. Sequences of the simulated oligomers ("γ" denotes L-Ser substitution at the $C\gamma$ ($C2'$) position) are shown in (c).

O-MeRNA modification can be found in naturally occurring RNAs¹⁸ and, though chemically quite simple (methylation of 2' ribose oxygens), this change significantly influences the chemical and physical properties of the derivatized oligonucleotide. Perhaps most importantly, the modified nucleic acid is more resistant to enzymatic degradation than the corresponding unmodified RNA.¹⁹ Also, methylation preferentially stabilizes the C3'-endo sugar pucker²⁰ that is characteristic of the canonical A-form double helix, and therefore facilitates binding to complementary RNA strands. Consistent with this stabilization, 2'-O-MeRNA/RNA heteroduplexes melt at relatively higher temperatures.^{21,22} Finally, of greatest relevance in terms of antibiotic design, 2'-O-MeRNA decamers have been shown to inhibit in vitro translation by *E. coli* 30S ribosomal extracts.¹⁵

The other oligomer of interest, PNA,²³ has emerged as a promising class of nucleic acid analogues over the past two decades.²⁴ In PNA, the negatively charged sugar-phosphate backbone is replaced by neutral peptidic units (Figure 1a,b). This unusual hybrid backbone contributes to the resistance of PNA to cellular proteases and nucleases.²⁵ The several NMR and crystallographic structures of PNA that have been determined confirm that PNAs bind complementarily to RNA and DNA to form either double (PNA/RNA,²⁶ PNA/DNA²⁷) or triple (PNA/DNA/PNA²⁸) helices. The exceptional thermal stability of PNA•nucleic acid complexes²⁹ can be attributed to the lack of electrostatic repulsion between the neutral PNA and charged nucleic acids backbones. Indeed, PNA can even bind to double-stranded DNA²³ or RNA³⁰ fragments, disrupting such structures via a so-called "strand invasion" mechanism. Of greatest

relevance in the present study, PNAs have also been shown to interact with bacterial 16S rRNA.¹⁷ Though PNA monomers and dimers conjugated to neamine did not enhance A-site binding affinity (versus neamine alone), other lines of evidence show that longer PNA sequences targeted at other regions of rRNA can effectively inhibit bacterial translation.^{14,30,31}

The nucleic acid-binding properties of PNA may be improved via backbone modifications.³² For instance, one such implementation, the introduction of an L-amino acid at the γ -carbon (atom $C2'$ in Figure 1b), was found to be particularly promising and relatively easy to synthesize. Circular dichroism and NMR studies of modified, single-stranded PNA oligomers show that L-Ser substitution induces formation of helical structure.³³ It was also found that the modification strengthens DNA- and RNA-binding by PNA; for that particular oligomer sequence (H-GCATGTTGA-Lys-NH₂, which differs from the PNA in the current work), substitution of all $C\gamma$ positions with L-Ser increased the melting temperatures of the heteromeric duplexes by 19 °C (DNA•PNA) or 10 °C (RNA•PNA).

Combined with experimental evidence for their interactions with 16S rRNA, the aforementioned features of 2'-O-MeRNA and PNA make them potentially valuable tools in designing antibacterial compounds. Elucidation of the physical properties (e.g., conformational dynamics) of these molecules would enable them to be used more effectively as modules for novel antibiotics, in particular, compounds that are more potent and less toxic (better sequence-specificity for bacterial versus eukaryotic ribosomal subunits). The intrinsic flexibility of these molecules as they exist immediately prior to binding a target

RNA (i.e., as single-stranded oligomers) remains relatively unexplored. As regards 2'-O-MeRNA, MD studies of the structural flexibility of double-stranded bulged 2'-O-MeRNA/ RNA complexes,³⁴ confirmed that 2'-O-MeRNA is more rigid than unmodified RNA. The only published MD study of single-stranded PNA³⁵ compared the dynamics of homomorphous PNA, DNA, and RNA decamers. However, those simulations sampled only brief (1–1.5 ns) time scales and used a rather confined simulation cell (31.5 Å × 31.5 Å × 41.5 Å). The simulations reported here were computed for longer (25 ns) time scales, thereby enabling more thorough conformational sampling. Also, we employed a unit cell of considerable size to avoid possible periodicity-induced artifacts.^{36,37}

2. Methods

2.1. System Selection, Construction, Starting Structures.

A total of eleven 25 ns MD simulations were computed with the systems falling into the six classes as shown in Figure 1c; four of the decameric molecules were PNA-based and the other two were RNA-based. In particular, we studied (i) two variants (containing either thymine or uracil) of unmodified PNA, (ii) two Ser-derivatized PNA backbones, and (iii) two RNAs of identical sequence (unmodified and 2'-O-modified backbones).

For each decamer, two starting conformations were chosen to preferentially sample either (i) coiled/disordered configurations (henceforth denoted as “extended” or *E*) or (ii) a stacked, regularly organized structure (denoted as “helical” or *H*). Because both PNA and 2'-O-MeRNA oligomers are known to form helical complexes with complementary RNA,^{21,26} we were interested in exploring the conformational stability of helix-like single-stranded forms. Reciprocally, we also simulated the dynamics of initially extended conformations in order to gauge their tendency to form more ordered, stacked, or helical structures. The sequence 5'UGUUAUCGACU3', complementary to the A-site region of 16S rRNA, was chosen based on the aforementioned experiments of Abelian et al.¹⁵ The PNA version of this decamer was considered in two forms: one (with uracil) to examine differences between PNA and 2'-O-MeRNA arising only from differences in backbone structure, and another variant (with thymine) to allow comparison to published experimental and theoretical data which describe (almost exclusively) thymine-based PNAs.

To study the influence of backbone modifications on the conformational stability and dynamics of PNA (see above), we also simulated two L-Ser-γPNAs based upon the same decameric sequence (Figure 1c). Again, two variants were constructed: one with all Cγ positions modified, and the other with a single Ser modification in the middle of the sequence, at C6 (Figure 1c). This single-Ser derivative was chosen because experiments have indicated that PNA helical structure may be induced with a N→C-terminal directionality.³³

Construction of each simulation system (Figure 1c) began by assigning atomic coordinates to generate starting structures. Representative examples of the two types of initial conformations, a roughly *A*-form “*H*”elical geometry and a nonhelical “*E*”xtended one, are shown in Figure 2a,b. The *A*-helix like structure of the RNA decamer was built with the nucgen program of AmberTools1.2.³⁸ Hydrogen positions were optimized in vacuo using the sander code from the Amber 9 package³⁹ with 8000 steps of steepest descent followed by 2000 steps of conjugate gradient energy minimization. The initial helical structure of 2'-O-MeRNA was created by adding methyl groups to the previously generated RNA model. The added atoms and all hydrogens were energy minimized (using the same

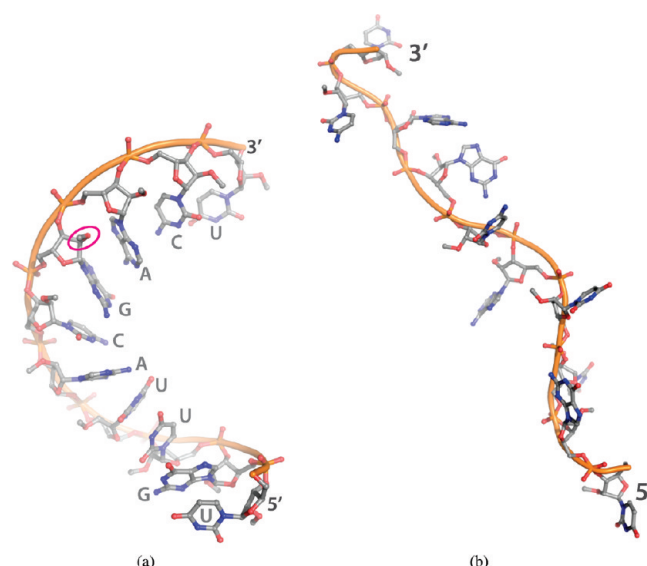


Figure 2. The 2'-O-MeRNA decamer in (a) helical and (b) extended initial conformations; the other oligomers were built into analogous starting structures prior to MD equilibration. For clarity, a single 2'-methoxy substituent is circled (magenta) in nucleotide G7 of panel (a).

method as above). To create the *A*-helix like conformation of the PNA(U) oligomer, the backbone atoms were removed from the initial helical RNA conformation, then backbone PNA units were added and minimized with nucleobase heavy atom positions restrained. In the second stage, the entire structure underwent unrestrained potential energy minimization. The initial extended conformation of RNA was taken from a high-temperature MD trajectory of A-Helical conformation. To obtain a starting structure for *E*-2'-O-MeRNA, methyl groups at 2'-*O* positions were added and minimized. The initial form of *E*-PNA was built by applying the same protocol as for its “helical” conformation. Both initial configurations of PNA(T) were prepared by adding methyl groups to uracils and further minimizing the added atoms and all hydrogens. Structures of L-Ser-γPNA were built based on PNA(T), with the C2' carbon replaced with L-serine. First, the additional atoms and, second, the entire structure were energy minimized.

2.2. Force Field Parameters. The topology and coordinate input files were prepared using the leap program from AmberTools1.2.³⁸ The simulations employed the parm99 Amber force field,⁴⁰ with the recent parmbsc0⁴¹ forcefield (modified α/γ backbone correlations) utilized for the RNA and 2'-O-MeRNA simulations. Partial atomic charges for the 2'-*O*-methyl groups in guanosine and cytidine in 2'-O-MeRNA were taken from the parameters contributed by Meyer & Case.⁴² The partial charges of the 2'-*O*-methyl groups of the remaining nucleosides (uridine, thymidine, adenosine) were assigned by analogy. PNA residues were given partial charges computed with the RESP method,⁴⁰ using the HF/6-31G* basis set, by Rathinavelan and Yathindra.⁴³ PNA backbone atoms were assigned the same types as in a previous MD study⁴⁴ employing the Amber force field, wherein the authors transferred them from standard peptidic fragments. Such an assignment can be justified by NMR studies⁴⁵ demonstrating that rotational energetic barriers for the amide bonds in PNA are similar to those observed in peptides. We used the TIP3P⁴⁶ water model and standard Amber Lennard-Jones parameters for monovalent ions (a radius of 1.868 Å and well depth of 0.00277 kcal/mol for Na⁺,⁴⁷ and corresponding values of 2.47 Å and 0.1 kcal/mol for Cl⁻).⁴⁸

2.3. Simulation Protocol. Each oligomer was immersed in a truncated octahedral box of explicit water. A minimal

clearance of atoms from the edge of the box of $\sim 19\text{--}20 \text{ \AA}$ (for extended) or $\sim 30 \text{ \AA}$ (for the A-helical structures) yielded boxes with similar final dimensions. The negatively charged RNA and 2'-O-MeRNA were neutralized by adding 9 Na^+ ions, replacing water molecules at positions of local minima of the electrostatic potential (tleap module of AmberTools 1.2³⁸). Next, equal numbers of Na^+ and Cl^- ions were added to every oligomer at random positions to yield ionic strengths of approximately 0.1 M. Each of the final MD simulation systems contained about 60 000 atoms.

Explicit solvent MD simulations were performed using NAMD 2.6⁴⁹ in the NpT ensemble with a constant pressure of 1 bar regulated by the Langevin piston method⁵⁰ and a constant temperature of 310 K ensured via the Langevin thermostat. Periodic boundary conditions were applied. To allow for a longer, 2 fs, integration time step, the SHAKE⁵¹ algorithm was used. For long-range interactions, the Particle Mesh Ewald method⁵² was applied with a grid spacing of about 1.0 \AA ; a 10 \AA short-range cutoff was used for nonbonded interactions.

The simulation protocol, taken from previous MD studies,^{53,54} was specifically designed and tested for nucleic acids. It consisted of four main phases. The first stage, thermalization, was performed in the NVT ensemble and consisted of two substages. During the first 65 ps, the temperature was linearly increased from 30 to 310 K with harmonic restraints of 50 kcal/mol/ \AA^2 imposed on the oligomer heavy atoms. Then, the restraints were relaxed to 25 kcal/mol/ \AA^2 , and the simulation continued for 35 ps. During the next phase, 300 ps of equilibration in the NpT ensemble, the restraints were gradually decreased starting from 5 kcal/mol/ \AA^2 to about 0, by reducing them by half after each 50 ps. The final equilibration phase (NpT) lasted 600 ps and was followed by a 25 ns production stage.

2.4. Data Analysis. The data from the entire (i.e., 25 ns) production phase of each MD trajectory were used for further processing and analysis. Geometric properties such as root-mean-square deviation (rmsd), distances, planar, and torsional angles were analyzed using ptraj (AmberTools 1.2³⁸) and VMD 1.8.7.⁵⁵ Unless otherwise noted, rmsd calculations were limited to nonhydrogen atoms. Pairwise rmsd matrices, composed of RMSDs between each pair of structural snapshots from the trajectories (sampled every 10th frame), were calculated after previous superposition of the heavy atoms of the molecules onto the structure from the first frame. The resulting rmsd values were presented in the form of a histogram. All data plots were generated with Gnuplot (v4.2) and Matlab (v7.5 R2007B).

MD conformations from each run were clustered with the kclust command of the MMTSB suite.⁵⁶ The method uses a stepwise optimal clustering algorithm based on a self-organizing neural net⁵⁷ to classify a set of conformations according to a specified time-series value. The Cartesian coordinate rmsd was chosen as a criterion for the clustering procedure. The cluster assignment was optimized such that every structure in each cluster lied within a predefined radius (5 \AA) of the centroid. The method is described in detail in CHARMM software documentation.⁵⁸

Radial distribution functions were calculated using ptraj with a 0.1 \AA grid spacing. To estimate sequential stacking interactions, distances between the centers of masses of nucleobase rings (neglecting hydrogens and exocyclic atoms) were measured. After initial tests and visual inspection of trajectories, a 5 \AA internucleobase distance was chosen as the upper cutoff limit for stacking interactions.

The average values and standard deviations for parameters characterizing ideal A-form helices (P–P distance, P–P–P angle, P–P–P–P dihedral angle, and decamer end-to-end distance) were calculated for the following set of helical RNA crystal structures from the PDB:⁵⁹ 157D, 1QC0, 1QCU, 259D, 406D, 1D4R, 310D, 413D, 435D, 466D, 377D, 420D, 255D, 434D, 464D, 472D.

3. Results and Discussion

3.1. Global Structural Fluctuations. The conformational diversity of an antisense oligomer strongly influences its ability to form complexes with structurally variable target RNAs. To quantify conformational changes along MD trajectories, we calculated root-mean-square deviations (rmsd) with respect to starting conformations. For all decamers starting in an extended/disordered (*E*) state, RMSDs vary significantly in the 8–14 \AA range (Figure 3). On the contrary, trajectories beginning from initially helical (*H*) states maintain helix-like conformations with average rmsd values in the range of $\sim 4.5\text{--}5.5 \text{ \AA}$.

RMSDs for both initially helical PNA(T) and PNA(U) decamers (Figure 3a) fluctuate in a range of about 4–8 \AA , with average values of 5.5 and 5.7 \AA , respectively. For the *H*-PNA(T) trace, the rmsd tends to switch abruptly between two plateaus (about 5 and 6.5 \AA). Three distinct rmsd changes are visible (around 4, 13, 16 ns), which separate time periods with relatively low rmsd fluctuations. In contrast, for *H*-PNA(U) significant rmsd changes occur more often, and intermediate rmsd values are also more frequently acquired. These observations are confirmed by pairwise rmsd histogram (see Methods) for the “helical” oligomers (Figure 4). The distribution for PNA(U) is slightly wider than for PNA(T), suggesting that PNA(U) can adopt a broader range of distinct conformational states on the time scale of our simulations. Additionally, the maxima of the distributions for both *H*-PNAs are shifted toward higher values (about 5 \AA) compared to RNA, implying that these decamers are more conformationally variable than “helical” RNA.

Comparison of pairwise RMSDs (Figure 4) for the “helical” forms of RNA and 2'-O-MeRNA decamers also suggests lower conformational variability of the latter; the rmsd peak of 2'-O-MeRNA is shifted to about 2 \AA and the distribution is narrower than for unmethylated RNA. Also, the rmsd plot in Figure 3b suggests that the *H*-RNA undergoes at least one distinct conformational change between 9 and 13 ns of the simulation, marked by a rise of rmsd from ~ 4.4 to 7 \AA . In contrast, the rmsd of 2'-O-MeRNA remains leveled during the entire 25 ns simulation with a standard deviation of only 0.6 \AA .

To assess RNA and PNA local flexibility on relatively shorter time scales, we computed fluctuations in rmsd for the “helical” oligomers along chosen 5 ns long simulation periods, the particular 5 ns windows being characterized by low rmsd fluctuations. The results demonstrate that the local flexibility of *H*-PNA(T) ($\Delta\text{rmsd}_{5\text{--}10 \text{ ns}} = 0.3 \text{ \AA}$) is lower than that of “helical” RNA ($\Delta\text{rmsd}_{15\text{--}20 \text{ ns}} = 0.6 \text{ \AA}$). This observation is in agreement with previous short MD simulations of single-stranded, homomorphous RNA, DNA, and PNA(T) oligonucleotides.³⁵ Those MD studies were carried out for a different sequence and in different conditions than in our work, that is, in rectangular boxes of smaller size ($31.5 \text{ \AA} \times 31.5 \text{ \AA} \times 41.5 \text{ \AA}$) and with the CHARMM^{60,61} forcefield. Despite these differences, the results are consistent; on relatively short time scales, the RNA oligomer exhibits greater local fluctuations than PNA.

3.2. Clustering Analysis. To determine the number of distinct conformations accessible to the oligomers, we clustered the MD-derived configurations using an rmsd-based method (see

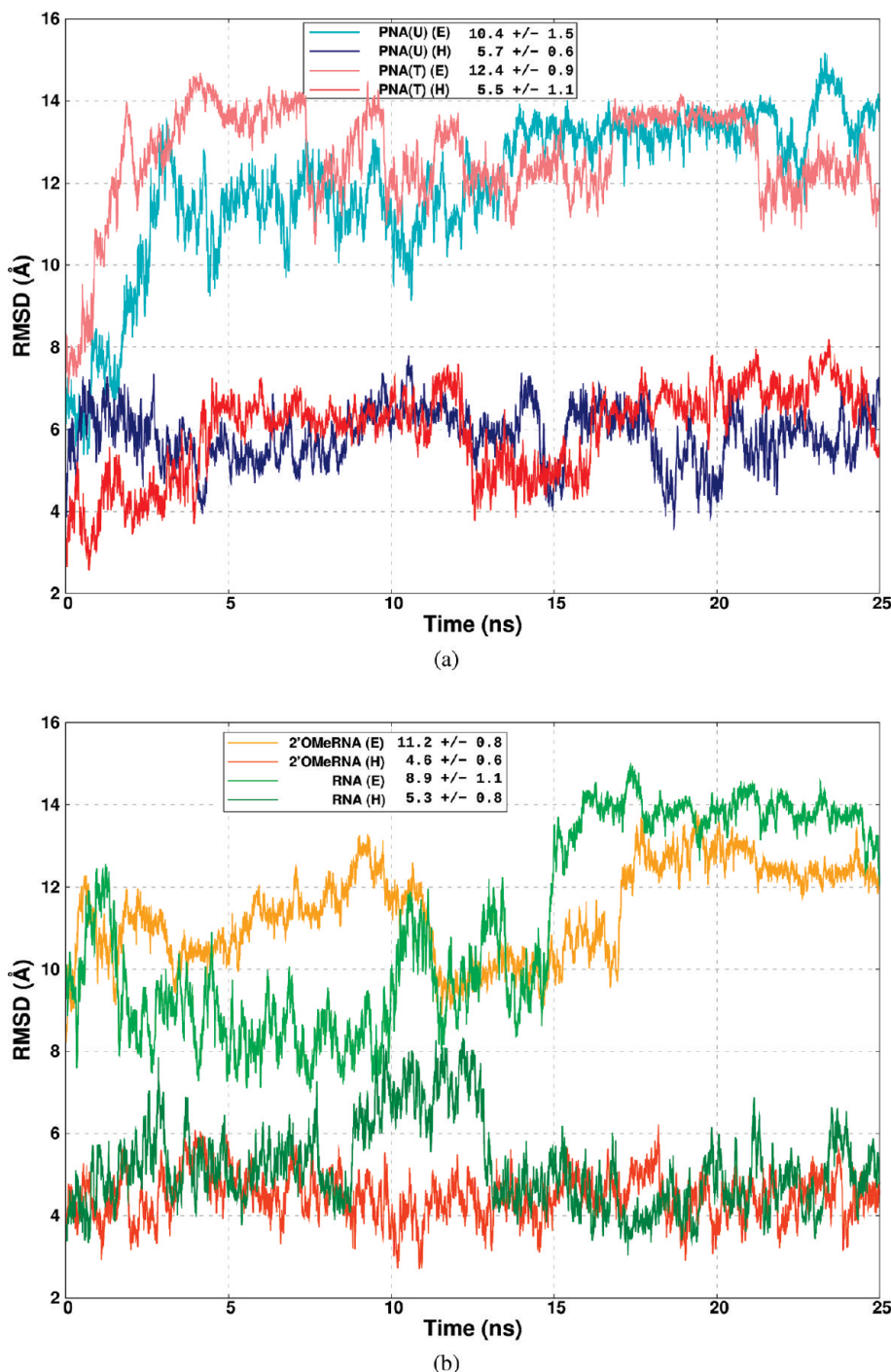


Figure 3. Time-series of rmsd values, referred to initial MD conformations, are shown for (a) PNA variants (U and T) and (b) unmodified RNA and 2'-*O*-MeRNA; the (E) and (H) labels refer to extended and helical starting structures, respectively, and the average rmsd values (in Å ± standard deviations) for each oligomer are provided in the inset legends.

Methods). The occupancies of all the resulting clusters are presented in Table 1, and representative structures for the one or two most occupied clusters are shown in Figure 5.

Clustering analyses, along with rmsd data, clearly show that the dynamical behavior of the initially helical oligomers differs from the “extended” counterparts. This dependence of MD-derived results on the initial configuration implies that the simulations have not fully converged: The 25-ns trajectories are apparently insufficient to sample the whole configurational space of these flexible oligomers. Limited sampling is mainly due to a large number of unrestrained rotational degrees of freedom, and energetic barriers that are too high for some conformational

transitions to occur on the nanosecond time scale (particularly in the case of the 2'-*O*-MeRNA oligomer). Regardless, from the perspective of using such oligomers as RNA binders, we are primarily interested in sampling near-helical configurations, as RNA frequently adopts such conformations under physiological conditions. In particular, our potential RNA target, the double-stranded A-site rRNA, also adopts such helical-like structures.

Looking more closely at clustering results, we note that conformations of both *E*- and *H*-PNA forms partition into the same numbers of structural classes, 7 and 4, respectively (see Table 1). The trajectories starting from extended conformations

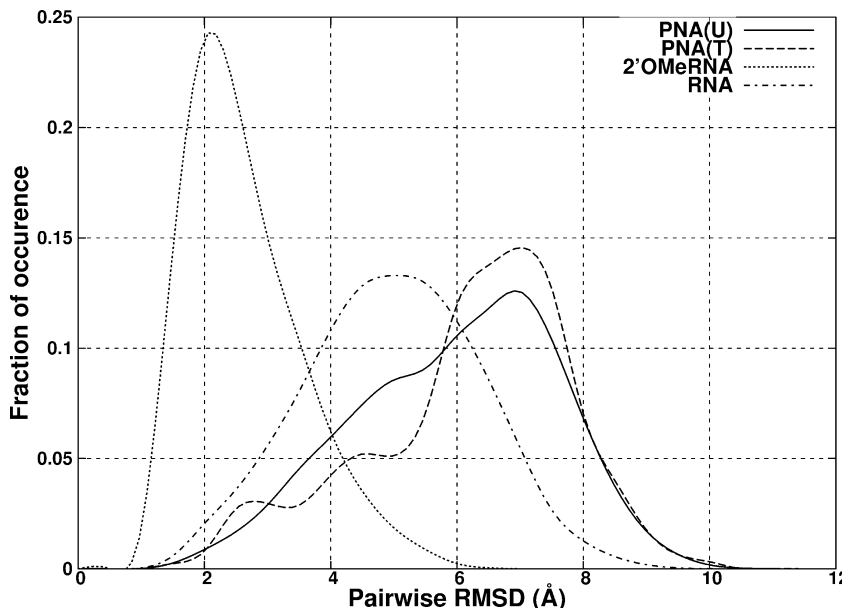


Figure 4. Pairwise RMSDs (computed between each pair of structures from the trajectory) for the PNA(U), PNA(T), RNA, and 2'-O-MeRNA systems are shown as histograms for trajectories that began from helical geometry.

TABLE 1: Relative Occupancies of Clusters Expressed As Percentages (Sorted in Decreasing Order) for (H)elical and (E)xtended Starting Conformations (Boldface Font Denotes the Representative Structures Shown in Figure 5)

		occupancies (%)
PNA(U)	(H)	30 , 19, 16 , 16, 9, 8, 2
	(E)	51 , 36, 9, 4
PNA(T)	(H)	25 , 24 , 16, 14, 13, 6, 1
	(E)	51 , 33, 9, 7
RNA	(H)	36 , 18 , 17, 15, 10, 5
	(E)	40 , 20 , 12, 11, 8, 7, 3
2'-O-MeRNA	(H)	100
	(E)	32 , 31, 22, 12, 3

converge to compact structural forms. The final, most populated (51% of the trajectory) conformation of the initially extended PNA(T) (Figure 5d) is stabilized by nucleobase T3•T4•A5 stacking interactions and is additionally “locked” by a stacked G2•T10 pair. *E*-PNA(U) (Figure 5e) predominantly exists in a looser conformation, featuring an exceptionally stable, nonsequentially stacked triplet of nucleobases (G7•C6•A8). The formation of such compact structures corroborates experimental studies on thymine-based PNAs that demonstrate that due to their hydrophobic nature PNA oligomers acquire compact and globular forms in solution.⁶²

The number of structural classes of the initially helical PNAs is higher than for their initially extended forms (Table 1). *H*-PNAs were not found to hydrophobically collapse (Figure 5a,b), potentially because the simulations were insufficiently long for breakage of initial, stabilizing stacking interactions. The most occupied clusters of *H*-PNA(T/U) correspond to extended, but almost fully stacked, helix-like structures; stacking is disrupted only at the termini (e.g., T1, C9, T10) or temporarily between middle nucleobases (Figure 5ab, left). Similar representative structures and equal cluster numbers suggest similarity in the dynamical behavior of both *H*-PNAs. However, if we use another criterion for comparison and count how often the structures from consecutive trajectory frames move from one particular cluster to another, it turns out that the conformation of PNA(U) is distinctly more variable (with 232 changes) than that of PNA(T) (154 switches). This suggests a greater confor-

mational variability of PNA(U) compared to PNA(T), and is consistent with previous experimental works demonstrating that replacement of uracils with thymines increases the thermal stability of nucleic acid duplexes.^{21,63,64} Our study implies that, in addition, thymines may have a conformationally stabilizing effect on single-stranded oligomers. On the basis of this finding, we can conclude that the increased stability of thymine-rich duplexes may partly arise from lower entropy loss upon binding of complementary oligonucleotides.

The two most occupied clusters of the *H*-RNA oligomer show that this RNA tends to preserve its helical structure (Figure 5e, right), or else adopts only partly unstacked conformations (left). It is known that a single-stranded RNA may adopt a helical conformation similar to an individual strand in a double-stranded RNA.^{65,66} Compared to its “helical” counterpart, *E*-RNA is quite flexible (Figure 5f, right), until it finally forms a rather stable compact conformation (left). Furthermore, we notice that the simulated structures of both RNA decamers are more structurally diverse than their 2'-O-MeRNA analogues. Whereas the *H*- and *E*-RNA partition into six and seven conformational clusters, respectively, *E*-2'-O-MeRNA yields five clusters (the most occupied one is shown in Figure 5g), and the “helical” 2'-O-MeRNA only one cluster (see Figure 12b). Increased structural rigidity of 2'-O-MeRNA presumably stems from the steric hindrance of the methyl group at the 2'-O position; this effect also contributes to the exceptional conformational stability of the “helical” 2'-O-MeRNA,⁷ which is the least dynamic of the simulated systems. Interestingly, the *E*-2'-O-MeRNA exhibits much larger conformational diversity (see Table 1) combined with almost complete absence of sequential stacking (Table 2, see the discussion below).

3.3. Backbone Flexibility. To compare the conformations adopted by the entirely dissimilar PNA and 2'-O-MeRNA or RNA backbones, we measured distances between the termini of the oligomers. We also monitored the distances, planar and torsional angles defined by neighboring linkage nitrogen (N4') and phosphorus (P) atoms, respectively (see Figure 1 for atom names).

Histograms of end-to-end distances of the “helical” PNA(U) and PNA(T) oligomers (Figure 6) reveal almost identical, very

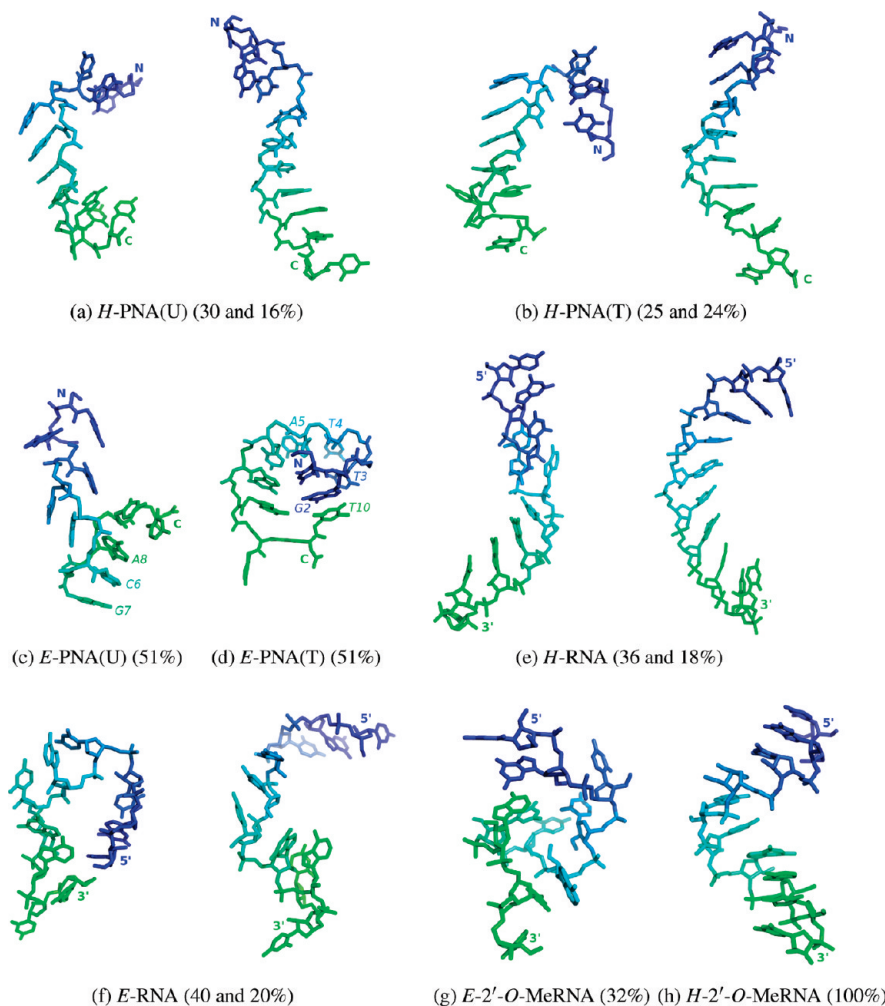


Figure 5. Representative structures are shown for the most populated regions of the conformational space of PNA variants (a–d), RNA (e,f), and 2'-O-MeRNA (g,h); these structures are “representative” in the sense of lying closest to the centroid of rmsd-based clusters. Occupancies of each cluster are provided in parentheses (see also Table 1). For clarity, the decamers are color-ramped from the first (blue) to last (green) residue; and any significant structural features mentioned in the text are indicated.

TABLE 2: Sequential Stacking—Percentage of MD Trajectory Time When Neighboring Bases Are Stacked^a

	U-G	G-U	U-U	U-A	A-C	C-G	G-A	A-C	C-U	avg	
2'-O-MeRNA	(H)	92	92	87	89	99	95	98	99	95	94
	(E)	19	2	25	0	0	7	40	0	12	12
RNA	(H)	50	60	9	35	10	66	55	44	31	40
	(E)	47	64	5	81	35	0	42	8	13	33
PNA (T)	(H)	54	90	32	68	82	74	94	9	12	57
	(E)	79	17	8	60	97	80	77	0	5	47
PNA (U)	(H)	23	88	34	58	91	67	96	59	40	62
	(E)	0	11	4	55	4	90	0	0	60	25
10SerPNA	(H)	0	99	98	39	87	96	99	37	7	62
	(E)	92	88	0	94	98	69	88	11	72	68
1SerPNA	(E)	71	65	1	32	19	40	96	71	0	44
ave.		48	62	27	56	57	62	71	31	32	

^a Estimation of stacking time is based on the criteria described in Methods; (H) - helical, (E) - extended initial conformations.

broad distributions with distances between 10–40 Å. In contrast, *E*-PNA(T) and *E*-PNA(U) acquire compact conformations with these values between 10–25 Å. However, the distribution for *E*-PNA(T) has only a single, well-defined maximum, whereas *E*-PNA(U) has two maxima. This implies that the latter oligomer is more structurally variable and less rigid than the thymine-based one.

End-to-end distance distributions for “helical” 2'-O-MeRNA and RNA show one peak and are narrower than those of PNA. This is likely because of the fewer rotational degrees of freedom

in the ribonucleotide backbone versus the PNA backbone. Furthermore, *H*-2'-O-MeRNA is shorter than *H*-RNA with their end-to-end distances being ~30 and 37 Å, respectively (Figure 6a). The length of the *H*-2'-O-MeRNA is similar to that characteristic for canonical A-form RNA (27 ± 2 Å for a decamer).

Whereas end-to-end distances capture global backbone flexibility, the proximity of neighboring residues can provide information about local backbone conformation. Histograms of interphosphorus distances for 2'-O-MeRNA and RNA show a

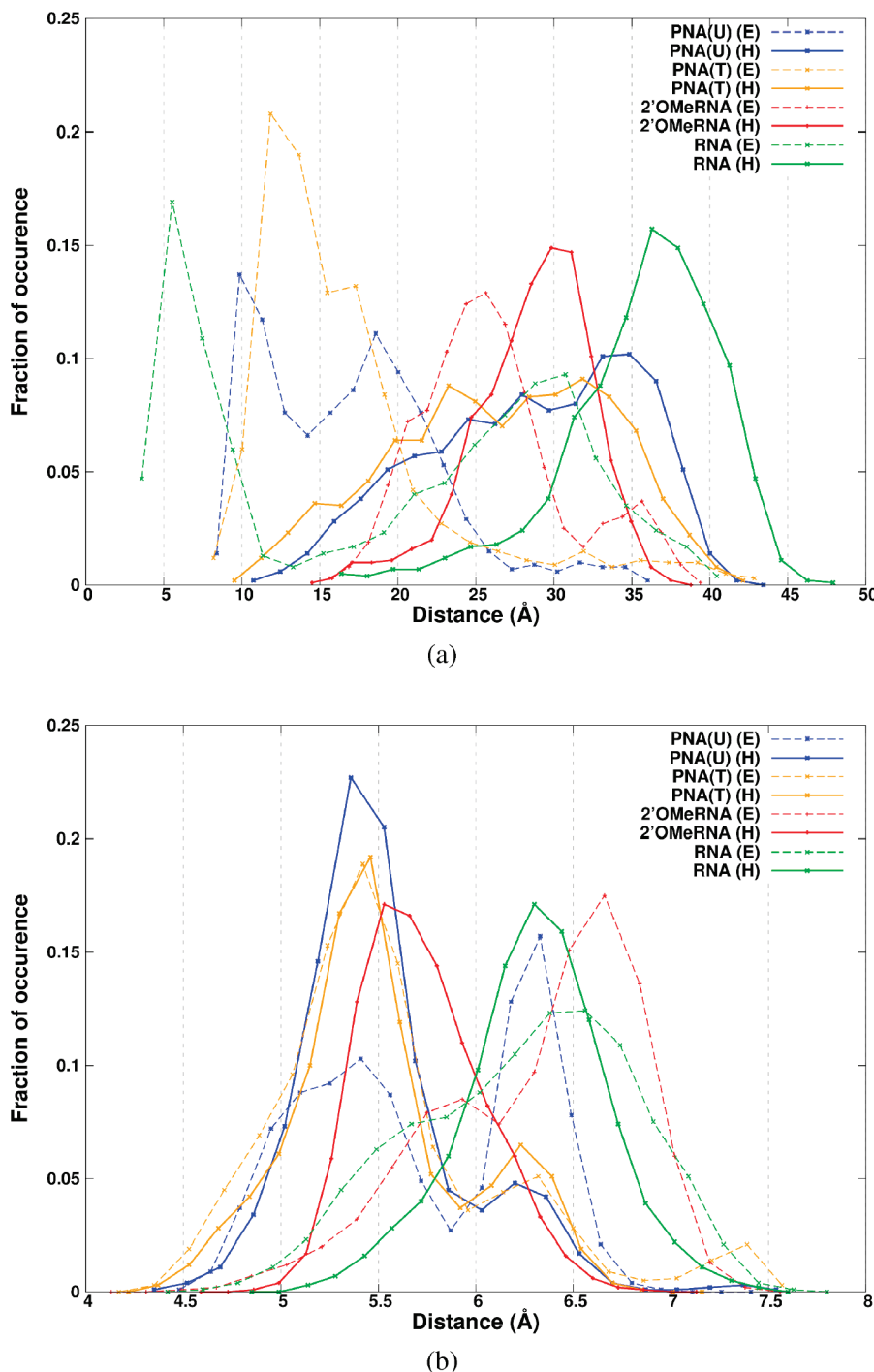


Figure 6. Distributions of global (a) and local (b) interatomic distances serve as reporters of backbone conformational variability. In (a), the global (end-to-end) distance is taken as $d(O5'\cdots O3')$ for RNA or 2'-O-MeRNA, and as the terminal N4'…N4' distance for the PNA systems; the value of this quantity is 28 Å for canonical A-form helices. The local measure (b) is defined as the distance between neighboring P (RNA) or N4' (PNA) backbone atoms, and equals 5.8 ± 0.2 Å for A-form RNA helices drawn from the PDB (see Methods). The aforementioned (E)xtended and (H)elical nomenclature is used in all figures.

well-defined, single maximum for the *H* forms (~ 5.5 Å [2'-O-MeRNA] and 6.3 Å [RNA]), but wide double peaks for the *E* forms (Figure 6b). The double maxima can be elucidated as different phosphate conformations occurring in the stacked and unstacked configurations adopted by neighboring nucleotides. The two forms of RNA have a similar main maximum for the P–P distance (~ 6.3 Å [“helical”] and 6.5 Å [“extended”]) but the 2'-O-MeRNA preferentially samples quite distinct conformations, with the initially helical structure displaying smaller inter-residue distances (~ 5.5 Å) than its “extended” counterpart (~ 6.7 Å). For PNA, the corresponding backbone distances

(N4'…N4') concentrate around two distinct maxima at ~ 5.3 and 6.3 Å (Figure 6b), indicating that at least two distinct backbone conformations are favorably adopted. Except for *E*-PNA(U), which primarily exhibits longer inter-residue distances of about 6.3 Å, all the distributions are similar with the most populated maximum at about 5.3 Å.

The peak in both *H*-PNA distributions lies toward lower inter-residue distances than in *H*-RNA (Figure 6b). Though this is the inverse of what was found in a previously simulated helical thymine-based PNA oligomer,³⁵ the starting configuration of PNA in the earlier work (*B*-form) is quite distinct (structurally

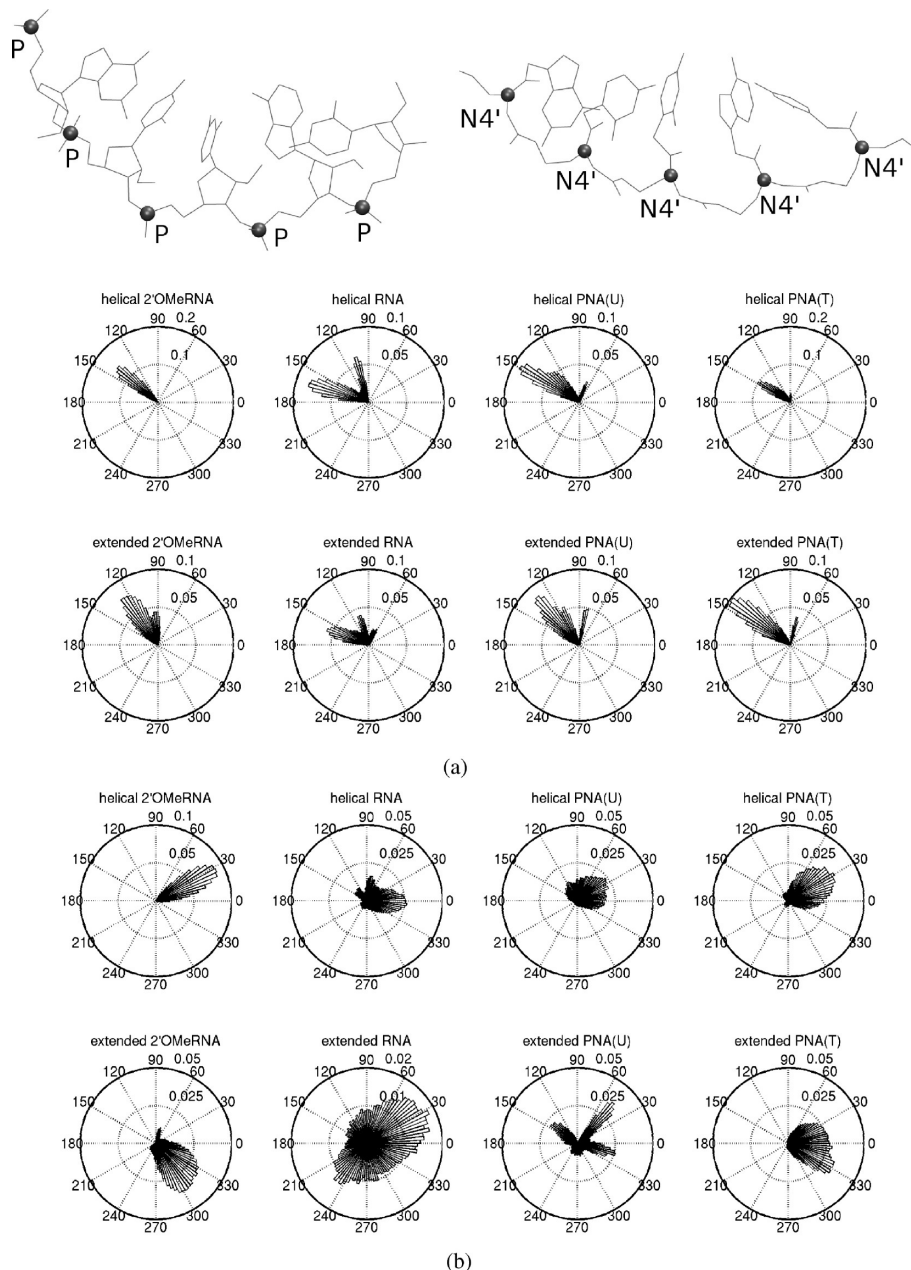


Figure 7. Histograms of angles defined by neighboring P (RNA and 2'-O-MeRNA) and N4' (PNA) atoms: (a) P—P—P/N4'—N4'—N4' and (b) P—P—P/P/N4'—N4'—N4'. These values calculated for a set of A-form RNA helices from PDB correspond to 150 ± 5 and $13 \pm 14^\circ$, respectively.

and dynamically) from the A-form helical initial configurations used here. This discrepancy suggests that observed differences in internucleobase distances may stem from choice of initial configurations, rather than a general tendency of PNA to adopt particular backbone conformations. Also, some of the discrepancies may arise from differences in (i) the precise simulation methods (forcefield parameters, boundary conditions, treatment of electrostatic interactions) and (ii) the time scales sampled (the MD simulations of Sen et al. were of shorter duration (~ 1.5 ns)).

Analysis of P—P—P/N4'—N4'—N4' planar angles (Figure 7a) indicates that the most rigid oligomer is the H-2'-O-MeRNA, which spans only a single, narrow range of angles ($\sim 140^\circ$), while the distribution of E-2'-O-MeRNA has a wider maximum ($\sim 120^\circ$). In contrast, all the other decamers exhibit more than one range of preferred values. Among PNA oligomers, there is a distinct difference in the angular distribution for E-PNA(U),

whose main maximum for the N4'—N4'—N4' angle is slightly shifted from $\sim 150^\circ$ (H-PNA) toward a lower value of $\sim 130^\circ$.

Angular histograms of P—P—P—P/N4'—N4'—N4'—N4' dihedral values (Figure 7b) illustrate that the backbone torsional freedom of PNA is similar in all the simulations and is not restrained to a narrow range of values; again, the only exception is that of E-PNA(U), which features three distinct ranges of preferred dihedral angles (centered about 50, 140, and 340°).

The sets of planar and dihedral angles differ significantly between RNA and 2'-O-MeRNA. The distributions are far broader for RNA, indicative of its greater conformational variability. The dihedral angles in H-2'-O-MeRNA ($\sim 15\text{--}45^\circ$) span a different and twice as narrow range of values as those of the corresponding “extended” structure ($\sim 280\text{--}340^\circ$). This indicates that on the ~ 25 ns time scale, the simulations of 2'-O-MeRNA with different initial configurations lead to dissimilar and non-interconvertible classes of conformers.

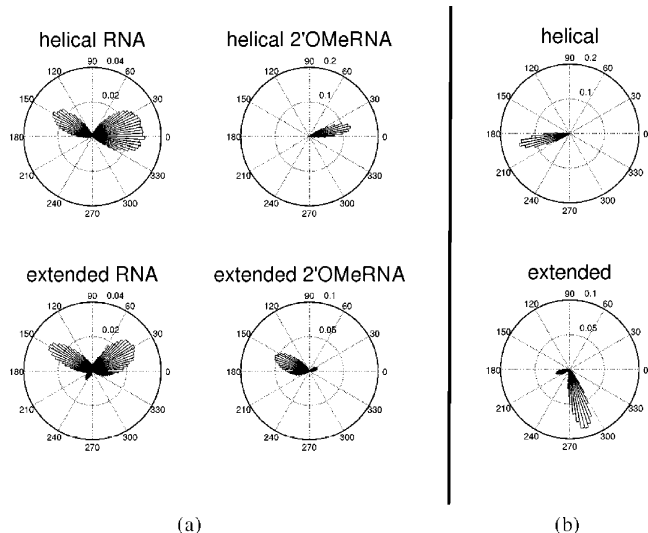


Figure 8. (a) Histogram of sugar pucker for 2'-O-MeRNA and RNA oligomers; (b) distribution of C3'-C2'-O2'-CM2 dihedral angle defining the position of the methyl group in 2'-O-MeRNA.

3.4. Comparison of RNA and 2'-O-MeRNA Backbone Conformation. The differential structural stability of “helical” RNA and 2'-O-MeRNA can be attributed to different factors. In particular, as demonstrated by previous NMR studies, in RNA duplexes the ribose hydroxyl group often engages in hydrogen bonds with solvent molecules, thus stabilizing the hydration shell.⁶⁷ MD simulations of the tRNA anticodon hairpin⁶⁸ also showed that, in this structured RNA, the 2'-OH group points preferentially toward O3', O4' (of the same ribose ring), or the nucleobase. In contrast, in our simulations the ribose hydroxyls in “helical” RNA are most often directed toward either O4' or O5' oxygens of the next ribose (with a C3'-C2'-O2'-HO2' dihedral angle of ~290°) and, less often, toward O3' (next ribose). This discrepancy may be explained by the fact that the single-stranded “helical” RNA oligomer does not preserve an ideal helical structure, acquiring instead a more extended conformation than that of the canonical A-form helix (see Figure 6a).

In regards to 2'-O-MeRNA, the only backbone hydrogen bond donor, the 2'O hydroxyl moiety, is methylated, and this precludes potentially stabilizing inter-residue hydrogen bonds involving backbone atoms. However, as noted above, the 2'O methoxy moiety can render the backbone more rigid. Previous theoretical work⁶⁹ suggests that this effect may arise from short-range van der Waals interactions between the methyl group and ribose ring; such forces effectively rigidify the 2'-O-MeRNA backbone, and also freeze-out much of the conformational variability that would otherwise be accessible to a backbone lacking the methyl substituent.

To analyze backbone conformational differences between RNA and 2'-O-MeRNA arising from 2'-O-methyl substitution, we measured the sugar pucker phase and C3'-C2'-O2'-CM2 dihedral angles. Sugar pucker geometry is generally quantified by the ribosyl pseudorotation angle (P), which adopts values of $P \approx -20\text{--}60^\circ$ (C3'-endo; typical of A-form helices) or $P \approx 120\text{--}200^\circ$ (C2'-endo; typical of B-form). In our trajectories, sugar pucker values of the H- and E-2'-O-MeRNA oligomers are almost exclusively either C3'-endo (see the $P \approx 15^\circ$ cluster in Figure 8a) or C2'-endo ($P \approx 160^\circ$ in Figure 8a) respectively, whereas for both unmodified RNAs the two P regions are nearly equally occupied. This result is consistent with the fact that sufficiently small substituents introduced at the 2'O position of

the ribose ring facilitate stabilization of A-form duplexes by enforcing C3'-endo puckers.⁷

In addition, the work reported here specifically implies that the 2'-methyl prevents interconversion between the two primary sugar puckers in 2'-O-MeRNA. For the dihedral angle C3'-C2'-O2'-CM2, only two well-defined values are sampled in the simulation (Figure 8b), and these correspond to the two possible sugar pucker conformations. In the E form of 2'-O-MeRNA (i.e., C2'-endo sugar pucker), the methyl group usually points toward the backbone (~285°), whereas in the H form (C3'-endo pucker) the preferred orientation of this methyl (~190°) is reversed and it points in the opposite direction (similarly as in the crystallographic (2'-O-MeRNA)₂ structure,⁷⁰ with a mean C3'-C2'-O2'-CM2 dihedral angle value of 192 ± 4°). In both simulated 2'-O-MeRNAs, all the sugar pucker conformations as well as 2' methyl positions remain the same as in the initial structures. Thus, the increased rigidity of the 2'-O-MeRNA backbone can be elucidated in terms of the steric hindrance due to a relatively immobilized methyl substituent.

3.5. Mobility of Bases. The dynamical properties of the bases in RNA or 2'-O-MeRNA, relative to the backbone, can be analyzed via the glycosidic torsional angle (χ). Figure 9a shows that, on average, the glycosidic angles for the “helical” RNA ($\chi \approx 270^\circ$, corresponding to the *high-anti* configuration) differs from that of 2'-O-MeRNA ($\chi \approx 200^\circ$, the *anti* region). Although χ values are more broadly distributed in the simulations of the “extended” oligomers, these also favor the *anti/high-anti* regions.

For PNA, we measured the C7'-C8'-N1/N9-C2/C4 dihedral angle (Figure 9b), which is analogous to the glycosidic angle of RNA and 2'-O-MeRNA. Both “helical” PNAs occupy a single well-defined angular region near 60°. The only distinct difference is that in the case of H-PNA(T) we observe an additional, but not frequently sampled, area around 150°. In terms of variance, the C7'-C8'-N1/N9-C2/C4 dihedral angles for “extended” PNA forms are as tightly distributed as for the “helical” forms because E-PNAs maintain stable compact structures over most of the trajectory.

However, the torsional mobility of PNA bases is not limited to only the C7'-C8'-N1/N9-C2/C4 dihedral angle. In the linker connecting the PNA backbone with bases, two other dihedral angles can be considered, C5'-N4'-C7'-O7' and N4'-C7'-C8'-N9(N1), that reflect the mobility of the nucleobases. The first angle describes the position of the side chain carbonyl group. Because of the peptidic nature of the methylene carbonyl linkage,⁴⁵ this carbonyl group may be located either *cis* to the backbone glycine (0°), or in the opposite, *trans* direction (180°). For the PNA starting structures, all residues were positioned in the first conformation, primarily because NMR studies of single-stranded PNA octamers⁴⁵ have revealed a substantial population of only one carbonyl conformer (the 0° one). These PNA backbone preferences are also seen in crystallographic structures.^{26–28} The starting configurations of these backbone torsion angles were maintained throughout the length of our trajectories (data not shown), as would be expected given the high free energy barrier for their *cis-trans* isomerization.

The other dihedral angle mentioned above describes rotation about the C7'-C8' bond. It is much less restrained and exhibits a broad range of allowed values between 180 and 270°; two primary maxima occur near 200 and 250° (data not shown). This additional degree of freedom decouples the mobility of PNA bases from backbone dynamics, and thereby severely lessens (relative to unmodified nucleic acids) correlations between bases and backbone atom fluctuations. In nucleic acids, the relatively rigid sugar ring rigidifies the backbone...base

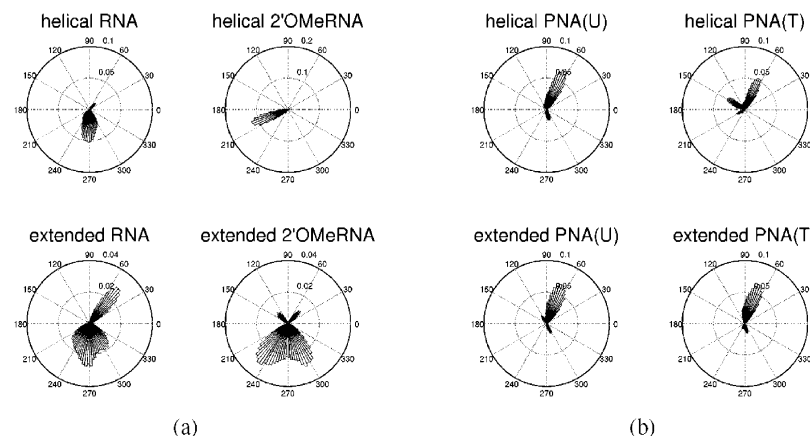


Figure 9. Distribution of glycosidic angle values (a) for 2'-*O*-MeRNA and RNA (defined as O4'-C1'-N1-C2 for pyrimidines and O4'-C1'-N9-C4 for purines), (b) for PNA(U) and PNA(T) (defined as C7'-C8'-N1-C2 for pyrimidines and C7'-C8'-N9-C4 for purines).

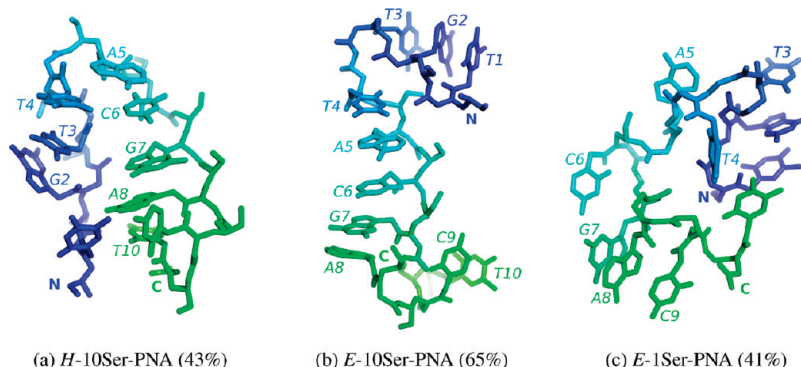


Figure 10. Representative structures from the most populated clusters of the three L-Ser- γ PNA trajectories are shown with occupancies indicated in parentheses.

linkage. This is in agreement with previously computed³⁵ correlation coefficients between RMSDs of the backbone and bases, which are significantly lower for PNA (0.38) than for DNA (0.92) or RNA (0.87).

3.6. Sequential Stacking. To characterize base-stacking interactions, we monitored the distances between the centers of mass of neighboring nucleobase rings (see Methods). Results from this approach are qualitatively consistent with those from quantum mechanical calculations of base–base interaction energies,⁷¹ demonstrating that stacking has a more stabilizing effect on neighboring purines than pyrimidines. Considering the sum–total of our simulations (100 ns), the most frequently occurring pair of bases is G7•A8, which is stacked 71% of the simulation time (this being the average across all eleven trajectories; see Table 2). The pyrimidine–pyrimidine pairs U3•U4 and C9•U10 are among the least stable doublets with stacking time fractions of 27 and 32%, respectively.

Experimental evidence suggests that adenine-rich RNA hexamers preserve, at least to some extent, a stacked/helical structure, even in single-stranded form.⁶⁶ Though our oligomers are not A-rich, our results comply with the experimental findings insofar as the RNA oligomer that began from a helical starting structure maintained stacking interactions for about 40% of the simulation, whereas its “extended” equivalent is stacked only 33% of the time (Table 2). Considering all the different “helical” decamers that were simulated, RNA appears to be the least stacked, while the modified oligomer *H*-2'-*O*-MeRNA is stabilized for exceptional lengths of time (~94% of the trajectory). The structure of *E*-2'-*O*-MeRNA persists in a much more unstacked, less ordered form during most of the simulation. There is no such difference between the two forms of the RNA

decamer; their stacking frequencies differ only slightly. This observation is consistent with the aforementioned influence of the methyl group in hampering conformational transitions of 2'-*O*-MeRNA.

For both *H*-PNAs, stacking occurs on average during similar ~60% fractions of the production phase (see Table 2). Indeed, data from UV melting experiments with PNA⁷² confirm base-stacking interactions in single-stranded oligonucleotides. In our simulations, the stacking time is longer for the “helical” form of PNA than for *H*-RNA. This can be attributed to the aforementioned low correlation between the mobility of the PNA backbone and bases;³⁵ PNA backbone flexibility minimally affects the dynamics of the bases and, therefore, does not disrupt sequential base-stacking interactions. Furthermore, higher stability of stacking in *H*-PNA containing thymines, versus RNA and DNA, has also been found in the earlier MD study of PNA.³⁵

3.7. Dynamical Behavior of L-Ser- γ PNAs. All PNA oligomers that incorporate L-Ser substituents were found to eventually converge to compact conformations (Figure 10), as occurred with the *E*-PNA(U) and *E*-PNA(T) oligomers, and as indicated in the plots of end-to-end distances (Figure 11). *H*-10Ser-PNA drifts away from canonical helical structure at ~8 ns, due to breakage of sequential stacking interactions between T4 and A5, and resulting in two separate blocks of stacked bases. However, it is intriguing that stacking within two groups of residues, G2•T3•T4 and C6•G7•A8•T10, is preserved over the course of the entire trajectory (Figure 10a). The initially unstacked *E*-10Ser-PNA structure collapses into two sequentially stacked blocks (T1•G2•T3 and T4•A5•C6•G7•A8•C9) near the beginning of the trajectory. These segments evolve to final stacks comprised of T1•G2•T3, T4•A5•C6, G7•A8, and C9•T10 tuples

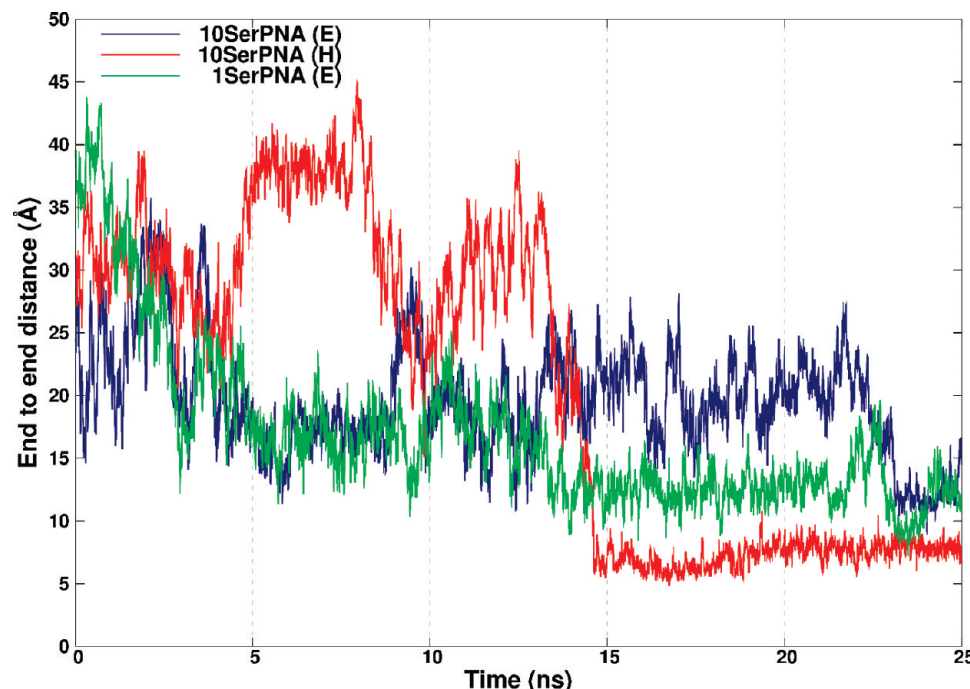


Figure 11. Time-evolution of the end-to-end distance for the three L-Ser-; as in Figure 6, the distance is defined between N4' atoms of the termini.

and, after about 23 ns, the structure acquires a more compact “S”-shaped conformation (Figure 10b), as evidenced by the dip in the black trace in Figure 11.

Although the conformations of both 10Ser-PNAs do not remain helical in the course of the simulations, we found that sequential stacking occurs here more frequently than for unmodified thymine-based PNA oligomers (Table 2). The two forms of 10Ser-PNA are stacked on average over 60% of simulation time, which is longer than for unmodified PNA(T), especially in its “extended” form (47%). Also, for both simulated 10Ser-PNA oligomers more nucleobase pairs have high stacking percentage times than other PNAs. If we assume an 80% cutoff, we can count five pairs satisfying that criterion for 10Ser-PNAs, and only up to three for the PNA(U/T) oligomers. For unmodified PNA(U/T), stacking often occurs with frequency near 50%. This suggests that L-Ser modification hinders the conversions between stacked and unstacked states.

In the case of “extended” 1Ser-PNA (for a representative final conformation, see Figure 10c), the stacking is comparable to E-PNA(T). However, we observe that three bases (G7•A8•C9) neighboring the serine derivatized C6 in the C-terminus direction are more frequently stacked than in the simulations of unmodified E-PNAs (Table 2). Moreover, the preceding three bases (T3•T4•A5) are exceptionally rarely stacked. This confirms a stabilizing effect of L-Ser substitution in the C-terminal direction,³³ and suggests a destabilizing influence of this modification on nucleobase stacking toward the N-terminus.

3.8. Interactions with Solvent. To analyze interactions of oligonucleotides with bulk solvent, we computed radial distribution functions of water molecules and ions around the phosphate oxygens of RNA and 2'-O-MeRNA, and around the carbonyl backbone oxygen O1' of PNA (upon superimposing their initial helical structures, this PNA oxygen is located in a similar position as the phosphate oxygens of RNA). Our results demonstrate that the methyl group of 2'-O-MeRNA does not influence the water distribution around phosphate oxygens. However, consistent with the relatively poor solubility of PNA in water,⁸ we observed that the maximal density of water

molecules (at 2.2 Å) is roughly 2-fold lower for PNA than for RNA or 2'-O-MeRNA (data not shown). Though the peptide bonds of the PNA backbone have nonzero dipole moments, the negatively charged phosphate groups in RNA and 2'-O-MeRNA more favorably attract water molecules.

The electrostatic properties of PNA differ substantially from RNA and 2'-O-MeRNA. The electrostatically neutral PNA backbones essentially do not bind sodium ions (Figure 12), whereas the radial distribution functions show exceptionally high densities of Na⁺ around the phosphate oxygens of “helical” 2'-O-MeRNA. The chief maxima of the distribution, near 2.3 and 4.5 Å, correspond to Na⁺ counterions interacting either directly, or through one water molecule, with backbone oxygens. These maxima are significantly higher for the well-ordered “helical” 2'-O-MeRNA than for its “extended” counterpart, or for either of the RNAs. The density of ions depends on the position of phosphates in the oligomer sequence; the inset in Figure 12 shows that regions of highest Na⁺ density are located near the central phosphates. The persistently stable 2'-O-MeRNA helix creates a kind of cleft surrounded by phosphate oxygens, and site-specifically bound Na⁺ ions partially neutralize the local build-up of negative backbone charges. This resultant decrease of repulsion between the negative charges in oligonucleotide strands, upon complexation, may contribute to the relatively fast kinetics of 2'-O-MeRNA binding to RNA.²²

4. Conclusions

We performed and analyzed eleven 25 ns MD simulations of several decamers: RNA, 2'-O-MeRNA, PNA(U), PNA(T) and L-Ser-γPNA, based upon sequences complementary to the RNA adjacent to the ribosomal A-site of *E. coli*. Though the dynamical properties of PNA and 2'-O-MeRNA oligomers have been investigated in up to 5 ns long MD simulations,^{34,73,35,74} the work reported here offers insight into the dynamics of a suite of single-stranded RNA analogues on a much longer time scale, and for different sequences. Notably, the sequences we simulated differ from oligomers used in previous computational

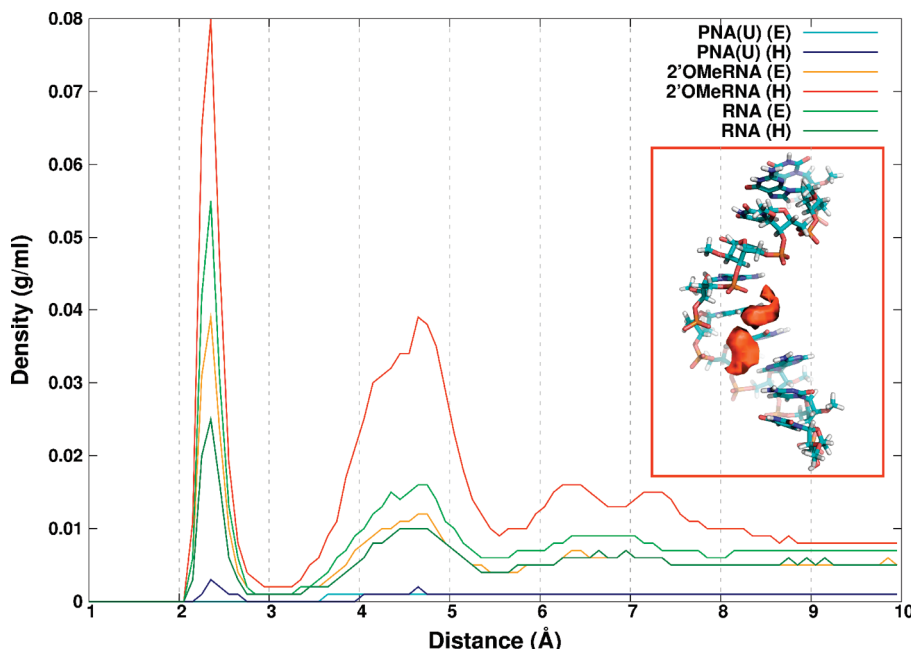


Figure 12. Radial distribution function of sodium ions around phosphate oxygens (RNA and 2'-O-MeRNA) or carbonyl backbone oxygen O1' (PNA(U)). Regions of highest sodium ion density near H-2'-O-MeRNA are shown in the inset (the isosurface represents an average density of 0.27 g/mL).

studies, and were chosen based on their biological and potential therapeutic significance as ribosomal A-site binders.

To the best of our knowledge, there exists no report of MD studies of PNA oligomers containing uracils. Analyses of rmsd patterns, end-to-end distances, and clustering results show that PNA(U) is more conformationally variable than thymine-containing PNAs, consistent with previous works showing that the thymine methyl group stabilizes nucleic acid duplexes.^{21,63} Therefore, one might expect the more flexible PNA(U) to be able to better adjust its conformation upon binding to an already structured RNA (e.g., a region of rRNA), though this would unfavorably elevate the entropic contribution to the binding free energy.

For all the initially extended forms of the modified and unmodified PNAs, we observe the formation of compact structures, presumably as a consequence of the hydrophobic nature of the PNA oligomer. We also find that the PNA backbone is more conformationally variable than the RNA and 2'-O-MeRNA backbones, consistent with its greater number of freely rotatable bonds. Additionally, we observe a stabilizing influence of L-Ser modification on the stacking properties of PNA, in agreement with experimental studies;³³ our L-Ser- γ PNA simulations confirm the N- to C-terminus directionality of that effect.

Methylation of the RNA backbone at the 2'*O* position substantially alters its dynamical properties. The rigidity of 2'-O-MeRNA was found to be increased compared to RNA, corroborating previous MD studies.³⁴ The “helical” conformation of 2'-O-MeRNA persists in an exceptionally stable structure with very rare unstacking events, while the “extended” form remains almost continually unstacked. The “helical” structure also exclusively shows the C3'-endo sugar pucker characteristic of A-form RNA, in contrast to the pure C2'-endo of the extended/disordered form. C2'-endo \leftrightarrow C3'-endo transitions did not occur in our simulations, and the low likelihood of such events implies the existence of an energetic barrier that is sufficiently high to prevent such interconversions on the time scale considered in this study. This suggests that the 2'-O-methyl group facilitates

creation of 2'-O-MeRNA/RNA complexes²² by reducing an unfavorable entropic contribution to the binding free energy, versus the RNA/RNA complex.

Interestingly, we also observed a distinctly higher density of Na⁺ ions around the “helical” 2'-O-MeRNA compared to the other oligomers, and particularly to its “extended” counterpart. This effect partially explains the fast hybridization of 2'-O-MeRNA probes with RNA;²² screening of backbone negative charges results in a reduction of the electrostatic repulsion between the two like-charged strands. In contrast, PNA essentially does not bind Na⁺ ions and, relative to RNA analogues, exhibits a relative depletion of water molecules in the vicinity of the backbone.

By examining the role of dynamics in potential antisense oligomers, our findings provide suggestions on how to modify such oligomers to make them more effectively bind various RNA motifs, many of which occur as irregular structures. Two opposing effects must be considered: structural adaptability of the oligomer is often a beneficial feature, yet a high degree of conformational flexibility results in a greater entropic penalty in the binding free energy. Thus, a goal is to find an optimal balance between the two extremes of (i) fixed shape, low entropic cost and (ii) flexible, adaptable structure but with unfavorable entropic contributions. To achieve that goal, we suggest that one may consider fine-tuning the antisense compound in terms of its dynamics, by designing RNA/2'-O-MeRNA/PNA/L-Ser- γ PNA hybrid molecules which adjust more efficiently to their targets. As an example, DNA/PNA⁷⁵ and RNA/PNA⁷⁶ chimeras have already been synthesized.

PNA oligomers prefer compact forms in solution. Therefore, reorganization of the oligomer is necessary for binding to a complementary helical RNA. As shown in this study, the addition of L-Ser- γ substituents is an effective way to structurally stabilize the PNA backbone and to enforce more ordered, better-stacked conformations. Also, our results suggest that the usage of PNA units with either thymines or uracils, as in the work of Mei et al.,¹⁷ could be considered as a way to preferentially stabilize/destabilize conformational states of PNA oligomers.

For RNA-based oligonucleotides, the addition of methyl or other alkyl groups at certain positions could be used to effectively restrict a selected region of RNA to a desired conformation. Additionally, our analysis of ion distributions suggests that, if one wants to make a 2'-O-Me-modified RNA oligomer more (or less) rigid, one could modify the phosphates in the middle of the molecule, making them localize sodium ions more (or less) strongly. This approach would offer a more subtle way to modulate the conformational and structural flexibility of this class of antisense compounds.

In conclusion, by elucidating the structural and physicochemical properties of potential antisense oligonucleotides, in terms of both intrinsic backbone dynamics and extrinsic factors (such as hydration or counterions), the work reported here may facilitate further efforts to design more efficacious antisense nucleic acids.

5. Abbreviations

MD, molecular dynamics; PNA, peptide nucleic acid; rRNA, ribosomal RNA; rmsd, root-mean-square deviation.

Acknowledgment. We acknowledge support from the University of Warsaw (ICM BST 1450/2009 and 1550/2010), Polish Ministry of Science and Higher Education (N N301 245236), Foundation for Polish Science (Focus program and Team project TEAM/2009-3/8 cofinanced by European Regional Development Fund operated within Innovative Economy Operational Programme), the University of Virginia, and the Jeffress Memorial Trust (J-971). Calculations were performed using resources at the University of Warsaw (Biomolecular Machines Laboratory and Grant G31-4, ICM) and the University of Virginia.

References and Notes

- (1) Wang, G.; Xu, X. S. *Cell Res.* **2004**, *14* (2), 111–116.
- (2) Lundin, K. E.; Good, L.; Strömberg, R.; Gräslund, A.; Smith, C. I. E. *Adv. Genet.* **2006**, *56*, 1–51.
- (3) Schiavone, N.; Donnini, M.; Nicolin, A.; Capaccioli, S. *Curr. Pharm. Des.* **2004**, *10* (7), 769–784.
- (4) Sinha, N. D.; Michaud, D. P. *Curr. Opin. Drug Discovery Dev.* **2007**, *10* (6), 807–818.
- (5) Mulamba, G. B.; Hu, A.; Azad, R. F.; Anderson, K. P.; Coen, D. M. *Antimicrob. Agents Chemother.* **1998**, *42* (4), 971–973.
- (6) Jepsen, J. S.; Sørensen, M. D.; Wengel, J. *Oligonucleotides* **2004**, *14* (2), 130–146.
- (7) Prakash, T. P.; Bhat, B. *Curr. Topics Med. Chem.* **2007**, *7* (7), 641–649.
- (8) Shakeel, S.; Karim, S.; Ali, A. *J. Chem. Technol. Biotechnol.* **2006**, *81* (6), 892–899.
- (9) Aboul-Fadl, T. *Curr. Med. Chem.* **2005**, *12* (19), 2193–2214.
- (10) Thompson, A. J. V.; Patel, K. *Clin. Liver Dis.* **2009**, *13* (3), 375–390.
- (11) Boulme, F.; Freund, F.; Moreau, S.; Nielsen, P. E.; Gryaznov, S.; Touleme, J. J.; Litvak, S. *Nucleic Acids Res.* **1998**, *26* (23), 5492–5500.
- (12) Sczakiel, G. *J. Hematother.* **1994**, *3* (4), 305–313.
- (13) Rasmussen, L. C. V.; Sperling-Petersen, H. U.; Mortensen, K. K. *Microb. Cell Fact.* **2007**, *6*, 24.
- (14) Good, L.; Awasthi, S. K.; Dryselius, R.; Larsson, O.; Nielsen, P. E. *Nat. Biotechnol.* **2001**, *19* (4), 360–4.
- (15) Abelian, A.; Walsh, A. P.; Lentzen, G.; Aboul-Ela, F.; Gait, M. J. *Biochem. J.* **2004**, *383* (Pt 2), 201–8.
- (16) Hermann, T. *Curr. Opin. Struct. Biol.* **2005**, *15* (3), 355–66.
- (17) Mei, H.; Xing, L.; Cai, L.; Jin, H.; Zhao, P.; Yang, Z.; Zhang, L.; Zhang, L. *Bioorg. Med. Chem. Lett.* **2008**, *18* (20), 5355–8.
- (18) Satoh, A.; Takai, K.; Ouchi, R.; Yokoyama, S.; Takaku, H. *RNA* **2000**, *6* (5), 680–6.
- (19) Cramer, H.; Pfleiderer, W. *Nucleosides, Nucleotides Nucleic Acids* **2000**, *19* (10–12, Sp. Iss. SI), 1765–1777.
- (20) Kawai, G.; Yamamoto, Y.; Kamimura, T.; Masegi, T.; Sekine, M.; Hata, T.; Iimori, T.; Watanabe, T.; Miyazawa, T.; Yokoyama, S. *Biochemistry* **1992**, *31* (4), 1040–1046.
- (21) Inoue, H.; Hayase, Y.; Imura, A.; Iwai, S.; Miura, K.; Ohtsuka, E. *Nucleic Acids Res.* **1987**, *15* (15), 6131–48.
- (22) Majlessi, M.; Nelson, N. C.; Becker, M. M. *Nucleic Acids Res.* **1998**, *26* (9), 2224–9.
- (23) Nielsen, P. E.; Egholm, M.; Berg, R. H.; Buchardt, O. *Science* **1991**, *254* (5037), 1497–1500.
- (24) Nielsen, P. E., Ed. *Peptide nucleic acids - protocols and applications*; Horizon Bioscience: Wymondham, U.K., 2004.
- (25) Demidov, V. V.; Potaman, V. N.; Frank-Kamenetskii, M. D.; Egholm, M.; Buchardt, O.; Sönnichsen, S. H.; Nielsen, P. E. *Biochem. Pharmacol.* **1994**, *48* (6), 1310–3.
- (26) Brown, S. C.; Thomson, S. A.; Veal, J. M.; Davis, D. G. *Science* **1994**, *265* (5173), 777–780.
- (27) Eriksson, M.; Nielsen, P. E. *Nat. Struct. Biol.* **1996**, *3* (5), 410–3.
- (28) Betts, L.; Josey, J. A.; Veal, J. M.; Jordan, S. R. *Science* **1995**, *270* (5243), 1838–41.
- (29) Hyrup, B.; Nielsen, P. E. *Bioorg. Med. Chem.* **1996**, *4* (1), 5–23.
- (30) Good, L.; Nielsen, P. E. *Proc. Natl Acad. Sci. U.S.A.* **1998**, *95* (5), 2073–2076.
- (31) Hatamoto, M.; Nakai, K.; Ohashi, A.; Imachi, H. *Appl. Microbiol. Biotechnol.* **2009**, *84* (6), 1161–1168.
- (32) Corradini, R.; Sforza, S.; Tedeschi, T.; Totsingan, F.; Marchelli, R. *Curr. Top. Med. Chem.* **2007**, *7* (7), 681–694.
- (33) Dragulescu-Andrasi, A.; Rapireddy, S.; Frezza, B. M.; Gayathri, C.; Gil, R. R.; Ly, D. H. *J. Am. Chem. Soc.* **2006**, *128* (31), 10258–10267.
- (34) Macchion, B. N.; Strömberg, R.; Nilsson, L. *J. Biomol. Struct. Dyn.* **2008**, *26* (2), 163–73.
- (35) Sen, S.; Nilsson, L. *J. Am. Chem. Soc.* **2001**, *123* (30), 7414–7422.
- (36) Hünenberger, P. H.; McCammon, J. A. *Biophys. Chem.* **1999**, *78* (1–2), 69–88.
- (37) Ye, X.; Cai, Q.; Yang, W.; Luo, R. *Biophys. J.* **2009**, *97* (2), 554–562.
- (38) Case, D. A.; Darden, T. A.; Cheatham, T. E., III; Simmerling, C. L.; Wang, J.; Duke, R. E.; Luo, R.; Crowley, M.; Walker, R. C.; Zhang, W.; Merz, K.; Wang, B.; Hayik, S.; Roitberg, A.; Seabra, G.; Kolossváry, I.; Wong, K. F.; Paesani, F.; Vanicek, J.; Wu, X.; Brozell, S. R.; Steinbrecher, T.; Gohlke, H.; Yang, L.; Tan, C.; Mongan, J.; Hornak, V.; Cui, G.; Mathews, D. H.; Seitun, M. G.; Sagui, C.; Babin, V.; Kollman, P. A. *Amber 10*; University of California: San Francisco, CA, 2008.
- (39) Case, D.; Cheatham, T.; Darden, T.; Gohlke, H.; Luo, R.; Merz, K. M. Jr.; Onufriev, A.; Simmerling, C.; Wang, B.; Woods, R. *J. Comput. Chem.* **2005**, *26*, 1668–1688.
- (40) Wang, J.; Cieplak, P.; Kollman, P. A. *J. Comput. Chem.* **2000**, *21* (12), 1049–1074.
- (41) Pérez, A.; Marchán, I.; Svozil, D.; Šponer, J.; Cheatham, T. E.; Laughton, C. A.; Orozco, M. *Biophys. J.* **2007**, *92* (11), 3817–29.
- (42) Meyer, T.; Case, D. Modified bases appearing in tRNA-phe from yeast from Contributed parameters on www.ambermd.org (accessed 20 Jan 2009).
- (43) Rathinavelan, T.; Yathindra, N. *FEBS J.* **2005**, *272* (16), 4055–70.
- (44) Shields, G. C.; Laughton, C. A.; Orozco, M. *J. Am. Chem. Soc.* **1998**, *121* (7), 1625–1625.
- (45) Chen, S.; Mohan, V.; Kiely, J. S.; Griffith, M. C.; Griffey, R. H. *Tetrahedron Lett.* **1994**, *35* (29), 5105–5108.
- (46) Jorgensen, W. L.; Chandrasekhar, J.; Madura, J. D.; Impey, R. W.; Klein, M. L. *J. Chem. Phys.* **1983**, *79* (2), 926–935.
- (47) Åqvist, J. *J. Phys. Chem.* **1990**, *94* (21), 8021–8024.
- (48) Smith, D. E.; Dang, L. X. *J. Chem. Phys.* **1994**, *100* (5), 3757.
- (49) Phillips, J. C.; Braun, R.; Wang, W.; Gumbart, J.; Tajkhorshid, E.; Villa, E.; Chipot, C.; Skeel, R. D.; Kalé, L.; Schulten, K. *J. Comput. Chem.* **2005**, *26* (16), 1781–1802.
- (50) Feller, S. E.; Zhang, Y.; Pastor, R. W.; Brooks, B. R. *J. Chem. Phys.* **1995**, *103* (11), 4613–4621.
- (51) Ryckaert, J.; Cicotti, G.; Berendsen, H. *J. Comput. Phys.* **1977**, *23* (3), 327–341.
- (52) Darden, T.; Perera, L.; Li, L.; Pedersen, L. *Structure* **1999**, *7* (3), R55–60.
- (53) Mura, C.; McCammon, J. A. *Nucleic Acids Res.* **2008**, *36* (15), 4941–55.
- (54) Romanowska, J.; Setny, P.; Trylska, J. *J. Phys. Chem. B* **2008**, *112* (47), 15227–43.
- (55) Humphrey, W.; Dalke, A.; Schulten, K. *J. Mol. Graph. Model.* **1996**, *14* (1), 33–8, 27–8.
- (56) MMTSB Tool Set; <http://blue11.bch.msu.edu/mmtsb/cluster.pl> (accessed 23 Oct 2009).
- (57) Karpen, M. E.; Tobias, D. T.; Brooks, C. L. *Biochemistry* **1993**, *32*, 412–420.
- (58) Clustering Time Series Data documentation. CHARMM c35b1. <http://www.charmm.org/documentation/c35b1/correl.html#%20Cluster> (accessed 1 Nov 2009).
- (59) Sussman, J. L.; Lin, D.; Jiang, J.; Manning, N. O.; Prilusky, J.; Ritter, O.; Abola, E. E. *Acta Crystallogr., Sect. D* **1998**, *54* (Pt 6 Pt 1), 1078–1084.

- (60) MacKerell, A. D.; Bashford, D.; Bellott, Dunbrack, R. L.; Evanseck, J. D.; Field, M. J.; Fischer, S.; Gao, J.; Guo, H.; Ha, S.; Joseph-McCarthy, D.; Kuchnir, L.; Kuczera, K.; Lau, F. T. K.; Mattos, C.; Michnick, S.; Ngo, T.; Nguyen, D. T.; Prodhom, B.; Reiher, W. E.; Roux, B.; Schlenkrich, M.; Smith, J. C.; Stote, R.; Straub, J.; Watanabe, M.; Wiórkiewicz-Kuczera, J.; Yin, D.; Karplus, M. *J. Phys. Chem. B* **1998**, *102* (18), 3586–3616.
- (61) MacKerell, A. D.; Banavali, N.; Foloppe, N. *Biopolymers* **2000**, *56* (4), 257–265.
- (62) Kuhn, H.; Demidov, V. V.; Coull, J. M.; Fiandaca, M. J.; Gildea, B. D.; Frank-Kamenetskii, M. D. *J. Am. Chem. Soc.* **2002**, *124* (6), 1097–1103.
- (63) Riley, M.; Maling, B. *J. Mol. Biol.* **1966**, *20* (2), 359–89.
- (64) Howard, F. B. *Biopolymers* **2005**, *78* (4), 221–229.
- (65) Johnson, W. C., Jr.; Tinoco, I., Jr. *Biopolymers* **1969**, *7*, 727–49.
- (66) Isaksson, J.; Acharya, S.; Barman, J.; Cherukuri, P.; Chattopadhyaya, J. *Biochemistry* **2004**, *43* (51), 15996–16010.
- (67) Conte, M. R.; Conn, G. L.; Brown, T.; Lane, A. N. *Nucleic Acids Res.* **1996**, *24* (19), 3693–3699.
- (68) Auffinger, P.; Westhof, E. *J. Mol. Biol.* **1997**, *274* (1), 54–63.
- (69) Yathindra, N.; Sundaralingam, M. *Biopolymers* **1979**, *18* (11), 2721–2731.
- (70) Adamiak, D. A.; Milecki, J.; Popenda, M.; Adamiak, R. W.; Dauter, Z.; Rypniewski, W. R. *Nucleic Acids Res.* **1997**, *25* (22), 4599–607.
- (71) Śponer, J.; Leszczyński, J.; Hobza, P. *J. Phys. Chem.* **1996**, *100* (13), 5590–5596.
- (72) Dueholm, K.; Nielsen, P. E. *New J. Chem.* **1997**, *21*, 19–31.
- (73) Terreux, R.; Pairet, S.; Cabrol-Bass, D.; Patino, N.; Condom, R. *J. Mol. Graph. Model.* **2001**, *19* (6), 579–85, 614–5.
- (74) Kaukinen, U.; Lönnberg, H.; Peräkylä, M. *Org. Biomol. Chem.* **2004**, *2* (1), 66–73.
- (75) Moggio, L.; Romanelli, A.; Gambari, R.; Bianchi, N.; Borgatti, M.; Fabbri, E.; Mancini, I.; di Blasio, B.; Pedone, C.; Messere, A. *Biopolymers* **2007**, *88* (6), 815–822.
- (76) Potenza, N.; Moggio, L.; Milano, G.; Salvatore, V.; Blasio, B. D.; Russo, A.; Messere, A. *Int. J. Mol. Sci.* **2008**, *9* (3), 299–315.

JP106404U